NAVAL POSTGRADUATE SCHOOL
MONTEREY, CALIFORNIA

THESIS

BIOMECHANICAL MODEL OF THE HUMAN THORAX FOR
IMPACT ANALYSIS

by

Timothy A. Hughes

September 1999

Thesis Advisor: Young W. Kwon

Approved for public release; distribution is unlimited.

19991126 102

REPORT DOCUMENTATION PAGE

Form Approved OMB No. 0704-0188

Public reporting burden for this collection of information is estimated to average 1 hour per response, including the time for reviewing instruction, searching existing data sources, gathering and maintaining the data needed, and completing and reviewing the collection of information. Send comments regarding this burden estimate or any other aspect of this collection of information, including suggestions for reducing this burden, to Washington Headquarters Services, Directorate for Information Operations and Reports, 1215 Jefferson Davis Highway, Suite 1204, Arlington, VA 22202-4302, and to the Office of Management and Budget, Paperwork Reduction Project (0704-0188) Washington DC 20503.

1. AGENCY USE ONLY *(Leave blank)*	2. REPORT DATE September 1999	3. REPORT TYPE AND DATES COVERED Master's Thesis

4. TITLE AND SUBTITLE: BIOMECHANICAL MODEL OF THE HUMAN THORAX FOR IMPACT ANALYSIS	5. FUNDING NUMBERS

6. AUTHOR(S) Hughes, Timothy A. LT/USN	

7. PERFORMING ORGANIZATION NAME(S) AND ADDRESS(ES) Naval Postgraduate School Monterey CA 93943-5000	8. PERFORMING ORGANIZATION REPORT NUMBER

9. SPONSORING/MONITORING AGENCY NAME(S) AND ADDRESS(ES)	10. SPONSORING/MONITORING AGENCY REPORT NUMBER

11. SUPPLEMENTARY NOTES
The views expressed here are those of the authors and do not reflect the official policy or position of the Department of Defense or the U.S. Government.

12a. DISTRIBUTION/AVAILABILITY STATEMENT Approved for public release; distribution is unlimited.	12b. DISTRIBUTION CODE

13. ABSTRACT *(maximum 200 words)* The Biomechanical response of the human thorax was studied using the finite element method by the classic stiffness method. The main focus was on validation of the model. The model was subjected to static and dynamic forces applied at the sternum. A plate was adhered to the sternum area and the model was subjected to a dynamic load to simulate an impact load similar to a projectile or bullet impact. The projectile characterized a 7.62 NATO M80 ball round. The bulletproof vest was similar in material properties to boron carbon composite. The results included the static analysis and transient analysis and the subsequent displacement due to the external loading. Stress was calculated from the displacements. The results were compared to earlier research and "live fire" tests conducted on cadavers.

14. SUBJECT TERMS Body Armor, Biomechanics, Thorax			15. NUMBER OF PAGES 62
			16. PRICE CODE

17. SECURITY CLASSIFICATION OF REPORT Unclassified	18. SECURITY CLASSIFICATION OF THIS PAGE Unclassified	19. SECURITY CLASSIFICATION OF ABSTRACT Unclassified	20. LIMITATION OF ABSTRACT UL

NSN 7540-01-280-5500

Standard Form 298 (Rev. 2-89)
Prescribed by ANSI Std. 239-18 298-102

BIOMECHANICAL MODEL OF THE HUMAN THORAX FOR IMPACT ANALYSIS

Timothy A. Hughes
Lieutenant, United States Navy
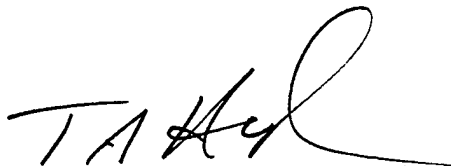Bachelor of Engineering, University of Mississippi, 1991

Submitted in partial fulfillment of the
Requirements for the degree of

MASTER OF SCIENCE IN MECHANICAL ENGINEERING

from the

NAVAL POSTGRADUATE SCHOOL
September 1999

Author: _____
Timothy A. Hughes

Approved by: _____
Young W. Kwon

_____
Matthew D. Kelleher, Acting Chairman
Department of Mechanical Engineering

ABSTRACT

The Biomechanical response of the human thorax was studied using the finite element method by the classic stiffness method. The main focus was in validation of the model. The model was subjected to static and dynamic forces applied at the sternum. A plate was adhered to the sternum area and the model was subjected to a dynamic load to simulate an impact load similar to a projectile or bullet impact. The projectile characterized a 7.62 NATO M80 ball round. The bulletproof vest was similar in material properties to boron carbon composite. The results included the static analysis and transient analysis and the subsequent displacement due to the external loading. Stress was calculated from the displacements. The results were compared to earlier research and "live fire" tests conducted on cadavers.

TABLE OF CONTENTS

ACKNOWLEDGMENTS

I would like to express my great appreciation to Professor Young W. Kwon for his support throughout this research. His dedicated guidance has significantly enhanced my education at the Naval Postgraduate School.

I would also wish to thank Dave Marco for invaluable time and guidance in overcoming the many hurdles I encountered in C programming skills.

There is no amount of thanks or acknowledgement I could offer my wife, Mariel, for her love and support during this entire endeavor.

I. INTRODUCTION

The human skeleton specifically the thoracic skeleton and its load carrying capabilities are of great interest in highway traffic safety, military applications, and sports applications. The missions undertaken in the United States Navy are changing as the Navy moves from the historic blue water operations of the cold war to the littoral mission requirements of today's ever changing world. The Navy ships have traditionally been the home as well as the immediate protection to our sailors in battle. As the Navy becomes involved in police and peace keeping missions such as drug interdiction, blockades, refugee intervention, and search and board missions required by national objections or United Nations Security Council resolutions, we will require our sailors to leave the safety of the ship to face would-be enemies. It is essential that Navy and Marine personnel be provided with the most advanced and technically innovative equipment available to ensure their safety and mission accomplishment.

This research is an effort to assist in the development of better personnel protective equipment (PPE), specifically bulletproof vests, to ensure the safety of sailors, marines, soldiers, and airmen. Specifically the research is aimed at developing a better bullet/knife-proof vest using advanced ceramics and composites. The objective is to model and simulate the biomechanical response of the human thorax outfitted with the prescribed (PPE) and exposed to an impact using the finite element method. The validation of the model is based on historical research already conducted as well as "live fire" testing conducted on cadavers. The focus will then be in the evaluation of injury potential of military personnel, in particular internal organ damage as a result of the deflection of the sternum and subsequent communication with the bullet and sternum fragments.

The military PPE used for this research is a boron carbide ceramic armor that is widely used in "live fire" experiments. The bullet selected for this study is the 7.62 NATO ball round because of the wide use around the world and it was also used in the "live fire" experiments.

II. BACKGROUND

A. BIOMECHANICAL BEHAVIOR OF BONE

This chapter describes the physical makeup of human bone and cartilage as well as the mechanical properties associated with compact and cortical bone. The bone and cartilage simulated in the finite element model geometrically and physically represent the spine and rib cage. These biomechanical materials make up the vast majority of the finite element model that represents the musculoskeletal structure of the thoracic lumbar spine including the rib cage.

In the study of engineering materials such as steel and alloys it is imperative to understand the mechanical properties of the material used in a structure. Mechanical properties include but are not limited to ultimate strength, yield point, Young's Modulus (modulus of elasticity) and Poisson's Ratio. All of which are important design considerations for the engineer. The mechanical behavior of a structure or member varies based on geometry, external forces, loading rate, and frequency of application of load. The engineer must interpret the perceived environment to enable him to select the correct material and optimize the mechanical structure.

The biomechanical or tissue engineer does not have the luxury of material selection in the modeling of bone tissue. The biomechanical material properties and behavior are just as important in understanding living tissue, mechanisms of failure, and modeling of human tissue. The engineer must couple the knowledge of the human tissue with the perceived environment. The engineer can then select the most appropriate material for the (PPE) and optimize the structure.

When examined under the microscope bone is considered a composite as shown by Hamm's 1969 adaptation of the bone as seen in Figure 1. The basic unit of the bone is called the Haversian system or osteon. Each osteon has a vein in the center. The blood vessels are connected by transverse channels called Volkmann's canals.
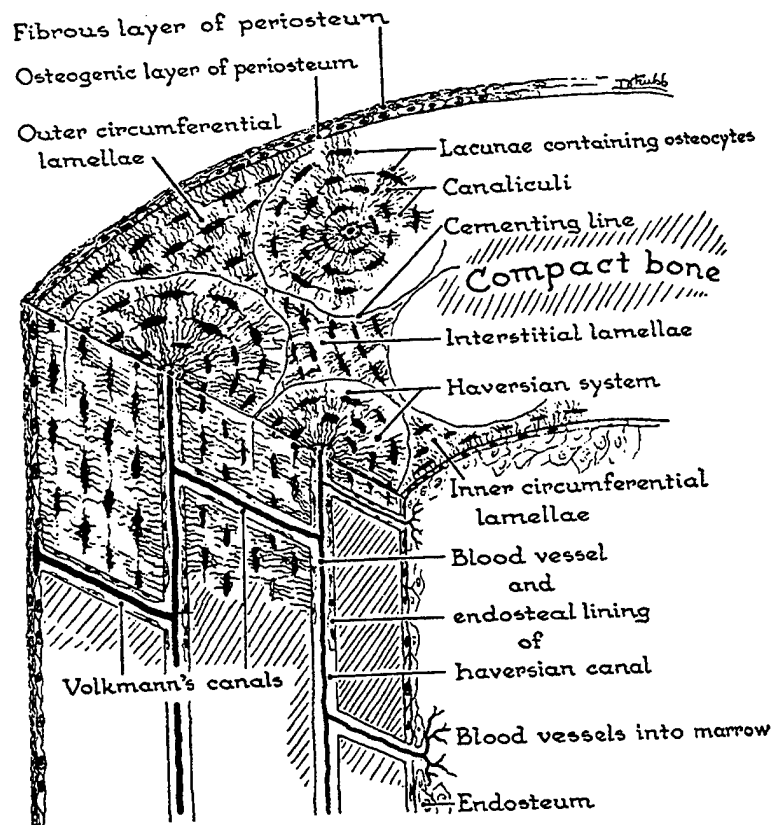
3

Fibrous layer of periosteum
Osteogenic layer of periosteum
Outer circumferential lamellae
Lacunae containing osteocytes
Canaliculi
Cementing line
Compact bone
Interstitial lamellae
Haversian system
Inner circumferential lamellae
Blood vessel and endosteal lining of haversian canal
Volkmann's canals
Blood vessels into marrow
Endosteum

Figure 1. Human Bone [Ref. 1]

Biomechanically bone may be considered a two-phase (bi-phasic) composite material. Minerals are one phase and collagen and ground substance make up the second phase, which is similar to fiberglass. Bone has similar characteristics to other composites in that strong brittle fibers are embedded in a weaker more ductile material or matrix. The most important properties of bone are its strength and stiffness. Load versus deformation curves similar to stress vs. strain curves allow for the tissue property determination such as ultimate tensile stress, yield point, and strain energy. This technique is similar to the strength of materials approach. Bone is considered a non-homogeneous anisotropic composite material. There are two types of bones, cortical and cancelleous or trabecular bone. Material and the material properties of bone differ

depending on the loading orientation. The mechanical properties of bone differ in the two types of bone. Cortical bone is stiffer than cancelleous bone. Cortex bone withstands greater stress but less strain than cancelleous bone when loaded to failure. Cancelleous bone in vitro (out of body) does not fracture until strain exceeds 75% but cortical bone fractures at strain levels as low as 2 % [Ref. 4]. The cancelleous porous bone structure has a greater capacity for energy storage.

A qualitative review of bone and other engineering material are shown in Figure 2. The stress strain curve shows bone exhibits a non-linear behavior and both ductile and brittle behavior. Since the structure of bone is different in the longitudinal and transverse direction it is expected to exhibit different material properties depending on the loading direction.
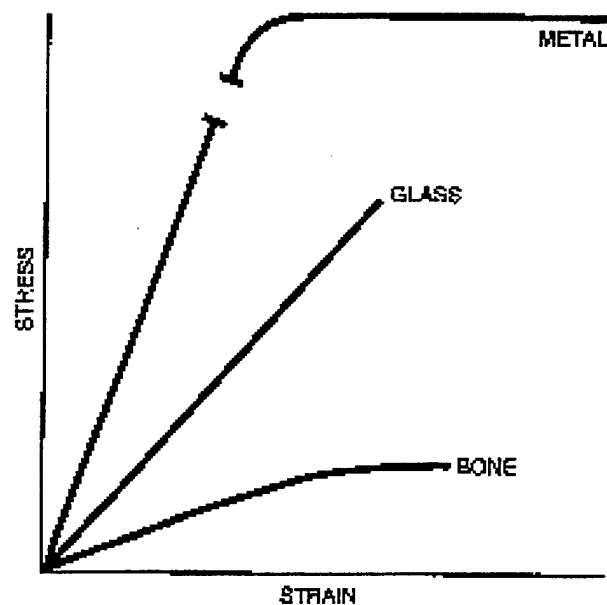

Figure 2. Stress Strain Curve for Bone [Ref. 2]

The metal and glass have a distinct linear elastic region where bone exhibits some plastic behavior even in the typical metals elastic regions. Bone also deforms less than metals after yielding. A microscopic investigation reveals the difference in biomechanical materials and metals that precedes failure in the two materials. Consider a

5

metal specimen in tension, yielding is produced by plastic flow and formation of slip planes in certain crystallographic directions that can be predicted based on the metal such as BCC, FCC, and HCP. Yielding is a result of dislocations of molecules in the lattice structure. Bone specimens, tested in tension, yields as a result of de-bonding of the osteons at cement line [Ref. 2]. Mechanical properties, geometry, loading modes, load rate, and frequency of applied load affect the behavior of bone subjected to external forces. Bone in vivo (in the body) is subjected to all types of loading including tension compression, bending, shear, and torsion. This study investigates the reaction of bone to applied loads. It is therefore important to establish an understanding of the fracture modes that may be seen.

Tension loading in bone produces maximum tensile stress on the plane perpendicular to the applied load. At the microscopic level, the failure mechanism for bone tissue loaded in tension is a result of de-bonding at the cement line and pulling out of the osteons similar to fiber pullout as seen in Figure 3 [Ref. 2].

Figure 3. Human Bone Loaded to Failure [Ref. 2]

Generally tension fractures are seen in cancelleous bone. Compressive loading results in bone structure shortening and widening. At the microscopic level the fracture mechanism for bone loaded in compression is oblique cracking of the osteons.

Compressive fractures are typically seen in the vertebrae in mature bone. In joints compressive failure is usually a result of abnormally strong contraction of the muscles surrounding the joint such as seen in patients undergoing electroconvulsive "shock" therapy. Shear is load applied parallel to the surface with deformation being internal angular shift of right angles. These right angles become obtuse or acute due to the shear loading. Shear fractures are typically seen in cancelleous bone [Ref. 2].

Bending is typically three point bending or four point bending. Since bone is asymmetric, tensile and compressive stresses may not be equal. The three point bending phenomenon is seen in boot top fractures where four point bending can exist between the hip and knee.

Bone loaded in torsion results in shear stresses distributed over the entire bone. The magnitude of the stress increases as the distance from the neutral axis increases. Maximum shear stresses act on a plane parallel to the neutral axis. Maximum tensile and compressive stresses act on planes diagonal to the neutral axis. In Figure 4 a torsional fracture of a canine femur is depicted where the short crack at the initiation site that extends parallel to the neutral axis represents shear failure. The crack extends at an angle of 30 degrees to the neutral axis and this is the plane of maximum tensile stress.
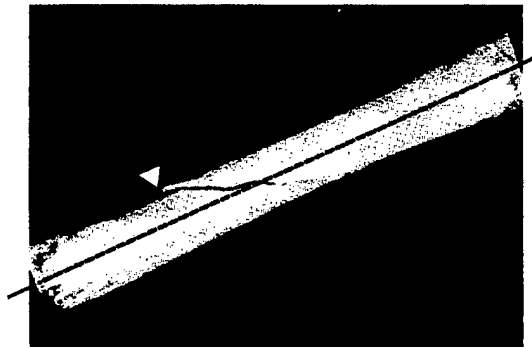

Figure 4. Torsional Fracture of Canine Femur [Ref. 2]

Bone unlike metals exhibit both brittle and ductile behavior depending on age. Mature bone is brittle in comparison to growing bone. A similar relation of ductile versus brittle behavior can be seen as a result of loading rate. An interesting result of

several studies shows that bone properties and behavior such as strength and stiffness is greatest if the orientation is the same as the loading orientation and direction exhibited in the body [Ref. 1]. Human tissue, particularly bone, has perfected the design optimization theories such as maximum stress and trajectory theory in that, bone material grows preferentially with maximum material in line with maximum force [Ref. 1].

B. BIOMECHANICAL BEHAVIOR OF CARTILAGE

COSTACARTILAGE OF THE RIB CAGE

The cartilage that attaches the bony ribs to the sternum is in the shape similar to the bony ribs and is called hyaline cartilage. Cartilage in the rib cage is responsible for the everyday ease at which the thorax moves to support respiratory functions. Hyaline cartilage is similar in both costacartilage and articular cartilage.

ARTICULAR CARTILAGE

The rib pairs articulate with the vertabrae via the costasternal joint and communicate with the sternum via cartilage. The costacartilage is articular cartilage and forms a joint referred to as costal articular facet. This joint allows a place for the head of the rib to articulate with the vertebrae as depicted in Figure 5. The joints that make up the costavertabral joints system are costal facet of transverse process, the inferior costal articular facet, superior costal articular facet, and a radiate ligament also depicted in Figure 5.

The human body has three types of joints. Fibrous joints are composed of fibers as the name implies. Cartilaginous joints are joints where bones are united by cartilage allowing only slight flexible movement. The costovertebral joints are these type of joints. The articulating bone ends are covered by a thin (1-5mm) dense white connective tissue called hyaline articular cartilage (a type of elastic cartilage that grossly appears smooth and semitransparent with a blueish-white tint. The articular cartilage is typically void of blood vessels, lymph channels, and nerves. The primary function of articular cartilage is to distribute the load over a wide area and to allow relative movement of the opposing joint surfaces with minimal friction and wear. The fiber bundles form a root

8

system that anchors the cartilage to the underlying bone. These fiber bundles are made up of collagen. The most important mechanical property of collagen is their tensile stiffness and strength. The size of a single collagen fiber prohibits individual testing to determine strength but this may be inferred by testing materials with large collagen content such as tendons [Ref. 2]. Tendons have a tensile stiffness of 10^3 MPa and a tensile strength of 50 MPa [Ref. 1]. Although strong in tension collagen is very weak or irresistant to compression because of the high slenderness ratio, which allows for ease of buckling under a compressive load. Articular cartilage is anistropic and as such its material properties differ with loading direction. The exact reason for the anisotropic behavior is unknown. Proteoglycans (PG's) are large protein-polysaccharide molecules that exist either as monomers, simple molecular units, or aggregates. PG monomers are made up of a core approximately 200nm long to which about 150 glycosaminglycan (GAG) chains are attached. These monomers make up several different types of PG aggregates depending on the bonding. The PG aggregates are not distributed evenly through the cartilage but are unhomogeneously dispersed throughout the articular cartilage. It is generally accepted that the PG aggregation promotes immobilization of the (PG's) within the collagen network adding structural rigidity to the extracellular matrix. Water is the most abundant component of the articular cartilage and is most concentrated near the surface. Water is found to decrease almost linearly with increasing depth into the matrix. Water contains many free mobile cations that influence the mechanical behavior of the cartilage. The fluid provides a transport medium that permits diffusion of gases, nutrients, and waste products between the chondrocytes and surrounding synovial fluid. Most of the water in the cartilage is extracellular and occupies the intermolecular space in the collagen fiber networks. The water is free to move when a load or pressure gradient is applied to the tissue. This movement is essential in the lubrication of the joint and the mechanical behavior of diarthrodial joints. Articular cartilage has two distinct phases, a fluid phase which consists of water with inorganic salts dissolved in solution and a solid phase which consists of the organic matrix. Articular cartilage is considered a fluid filled, porous-permeable medium with both solid and fluid phases and each distinct constituent of both phases playing a role in

9

the functional behavior of the cartilage [Ref. 2]. A human joint is exposed to varying degrees of force at the surface from near zero to several times body weight.
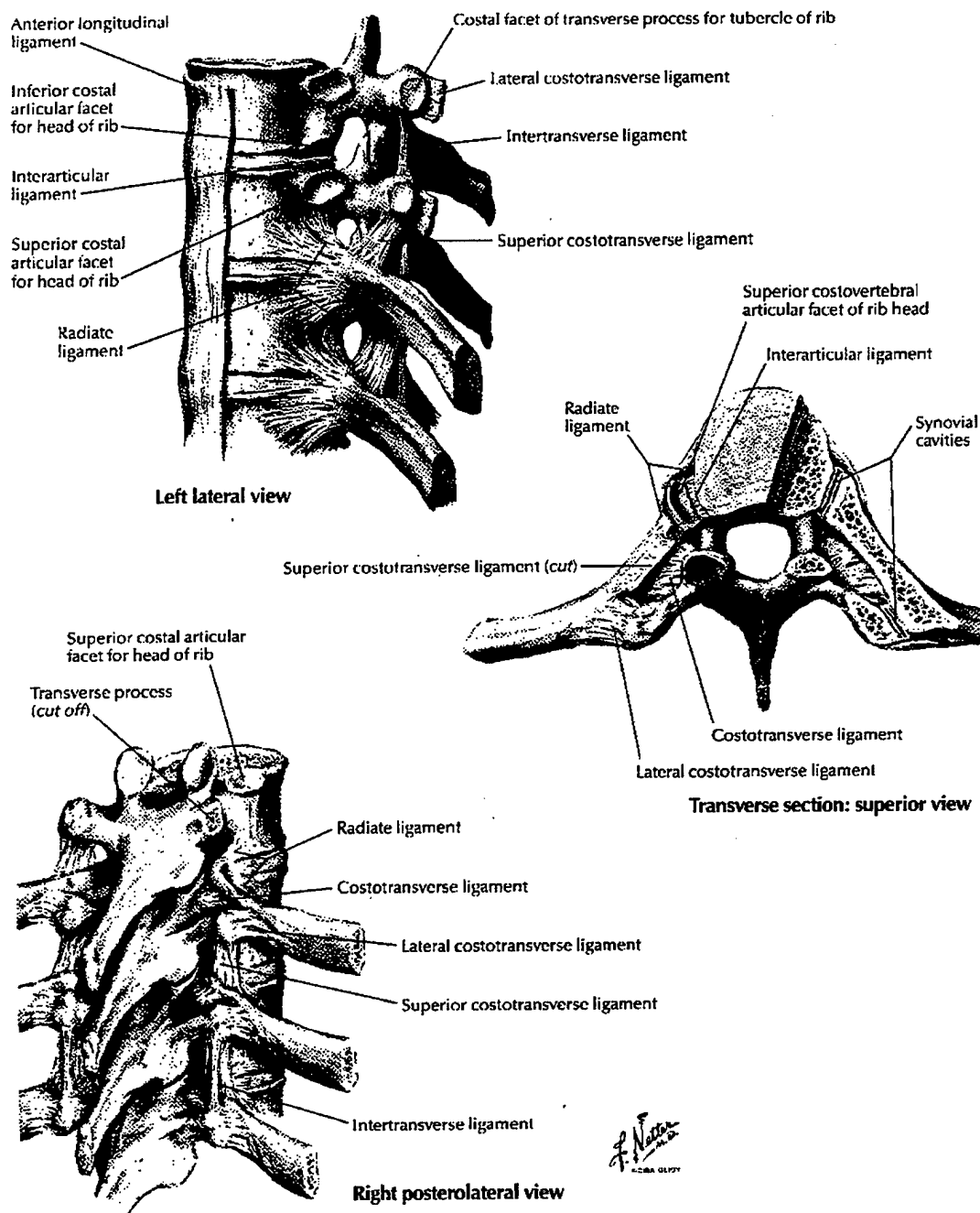

Left lateral view

Transverse section: superior view

Right posterolateral view

Figure 5. Costovertebral Joints [Ref. 3]

Under physiologic loading the articular cartilage is a highly stressed material.

If a material is subjected to a constant (time independent) load or constant deformation and the response varies with these loads, the material is said to be a viscoelastic solid. The two fundamental responses of a viscoelastic solid are creep and stress relaxation. Creep occurs due to constant load, where the response of the material is a rapid initial deformation followed by a slow progressively increasing deformation until equilibrium is reached. Stress relaxation occurs when the viscoelastic solid is subjected to constant deformation. The response is a high initial stress followed by a slow (time dependent) decreasing stress required to maintain the deformation.

Creep and stress relaxation are caused by internal friction due to motion of long polymer chains within the stressed material as in tendons and ligaments. The long-term viscoelastic behavior of bone is due to slip of the lamellae within the osteons along with the flow of interstitial fluids. The compressive viscoelastic behavior of articular cartilage is due to the flow of interstitial fluid. In shear it is primarily due to the motion of the long polymer chains of collagen and PG's. These two components of viscoelastic behavior in articular cartilage are known as biphasic viscoelastic behavior and flow independent or intrinsic viscoelastic behavior.

Biphasic creep in articular cartilage is caused by exudation of the interstitial fluid. Exudation is at first very rapid and diminishes gradually until flow ceases. During creep the applied load is balanced by the compressive stresses developed by the collagen-PG matrix and the drag developed by the flow of the fluid during exudation. In humans articular cartilage of 2 – 4 mm thick, experiencing creep reaches equilibrium in approximately 4 – 16 hrs. Cartilage of less than 1mm such as seen in rabbits takes about 1 hr. to reach equilibrium. Generally the time to reach equilibrium varies with the inverse of the square of the thickness [Ref. 2]. It is considered relevant to compare human cartilage to animals such as dogs and rabbits because experimentation has shown very similar results in material properties.

Stress relaxation is a result of an externally applied compressive load. The compressive load results in a stress rise followed by s stress relaxation. Stress rise in the compressive phase is due to exudation of the fluid and compaction of the solid material at the surface. Stress relaxation is due to relief or rebound of the compaction at the surface.

Under physiological loading conditions excessive stress levels are hard to maintain since stress relaxation quickly attenuates the stress [Ref. 1].

Both stress relaxation and creep can be used to determine permeability of the tissue. Permeability is a measure of the ease at which a fluid can flow through a porous permeable material. Permeability is inversely proportional to fluid drag exerted by the flowing fluid. Compaction of the solid matrix reduces porosity and the average hole diameter within the solid matrix and increases frictional resistance. The non-linearity of permeable material suggests that that tissue has a mechanical feedback. Under high loads the increased frictional drag against the interstitial fluid flow allows the tissue to appear stiffer and thus more difficult to allow exudation of the fluid [Ref. 1]. The behavior of cartilage as viscoelastic solids allows the cartilage to handle much larger loads and strain rates than predicted by a pure solid mechanics study.

C.   ANATOMY OF HUMAN THORAX

This chapter describes the general human skeleton including its material properties, connectivity, and movements. However, scapulars and arms are excluded for research purposes. Figure 6 shows the human skeleton and its anatomy.
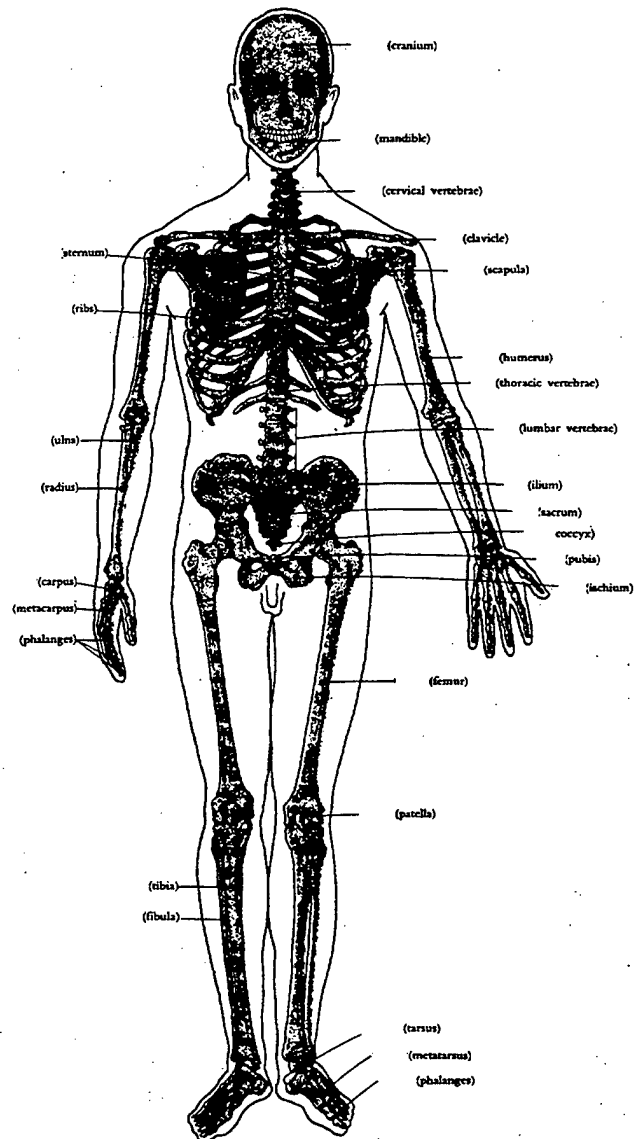

Figure 6. Human Skeleton (Anterior View) [Ref. 4]

1. Spine

The spine consists of 24 vertebrae, 23 discs and surrounding ligaments. It is divided vertically into three major sections; cervical, thoracic, and lumbar spines as shown in Figure 7. The upper seven vertebrae are called the cervical spine, known as neck, and give connection between the head and the trunk. In order to describe the unique location of each vertebra, a naming convention is used. The initial of each spinal name is combined with a number. That is, the uppermost cervical vertebra is called 'C1' and C2 is located right below C1. Figure 8 shows how two vertebrae are connected to each other. Each vertebra varies in dimensions depending on age, sex, and ethnic group. Another consideration is given to ligaments. Ligaments are uniaxial structures surrounding the vertebrae and they act like rubber bands. They then give resistance under tension but buckle when subjected to compression. The main function of ligaments is to allow proper spinal motion, without damaging the spinal cord and structure, and to support the vertebrae and trunk with muscle.

The disc is the inter-vertebral material with an anisotropic physical structure and viscoelastic property. It carries the compressive loading to the trunk along with the facet joints under the various forces and moments [Ref. 4]. Figure 9 shows a disc from the spinal column. The spinal cord is clinically an important component in the spinal column. This spinal cord is enclosed within the vertebral canal. In a mechanical perspective, however, it is not important and hence excluded in the spinal structure of this research.
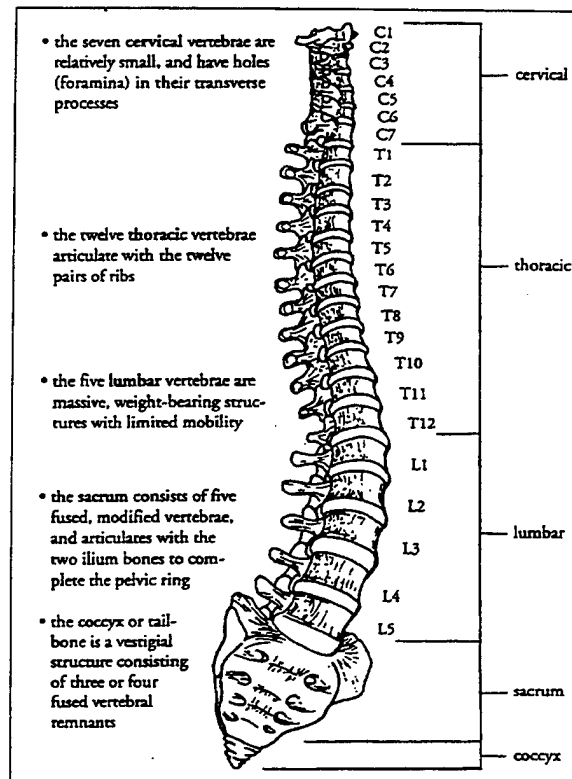
- the seven cervical vertebrae are relatively small, and have holes (foramina) in their transverse processes

- the twelve thoracic vertebrae articulate with the twelve pairs of ribs

- the five lumbar vertebrae are massive, weight-bearing structures with limited mobility

- the sacrum consists of five fused, modified vertebrae, and articulates with the two ilium bones to complete the pelvic ring

- the coccyx or tail-bone is a vestigial structure consisting of three or four fused vertebral remnants

C1
C2
C3
C4
C5
C6
C7 — cervical
T1
T2
T3
T4
T5
T6 — thoracic
T7
T8
T9
T10
T11
T12
L1
L2
L3 — lumbar
L4
L5
— sacrum
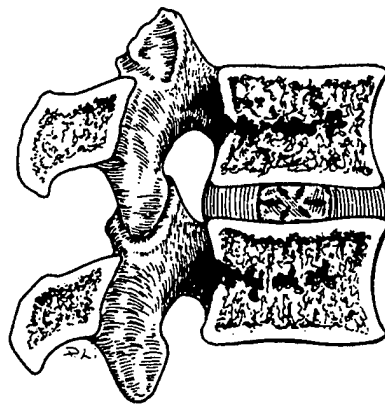— coccyx

Figure 7. Spinal Column [Ref. 5]

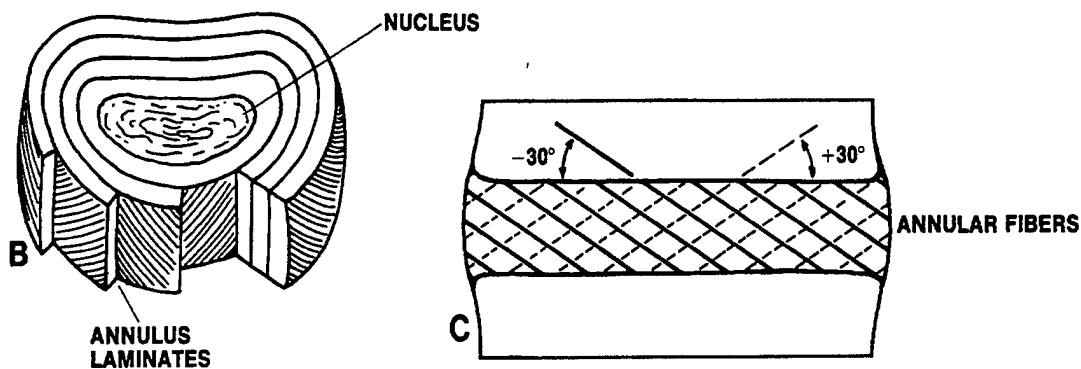**Figure 8. Connectivity of Two Vertebrae [Ref. 6]**

15

Figure 9. Intervertebral Disc [Ref. 5]

2. Ribs

The human thorax provides a structural body for the viscera. The structural body consists of the thoralumbar spine, and ribs that enclose the heart and lungs. The primary purpose of the thorax is to resist atmospheric pressure and to develop the required negative intrapleural pressure differential to permit normal flow of air in the lungs [Ref. 9]. The thorax also provides protection for the internal organs against injury. Ribs are elliptical in shape and vary in cross sectional area. The cross sectional properties including area and moment of inertia are largest at the sternochondral junction where the rib pairs articulate with the vertabrae and decrease proceeding into the shaft region to a minimum at the rib midpoint. The material properties increase in the region of the angle and decrease in the neck as the costal cartilage attaches to the sternum [Ref. 7]. As seen in Figure 10 the rib pairs are elliptical in shape with approximately fifty percent compact or cortical bone and the remaining marrow and cancelleous bone.
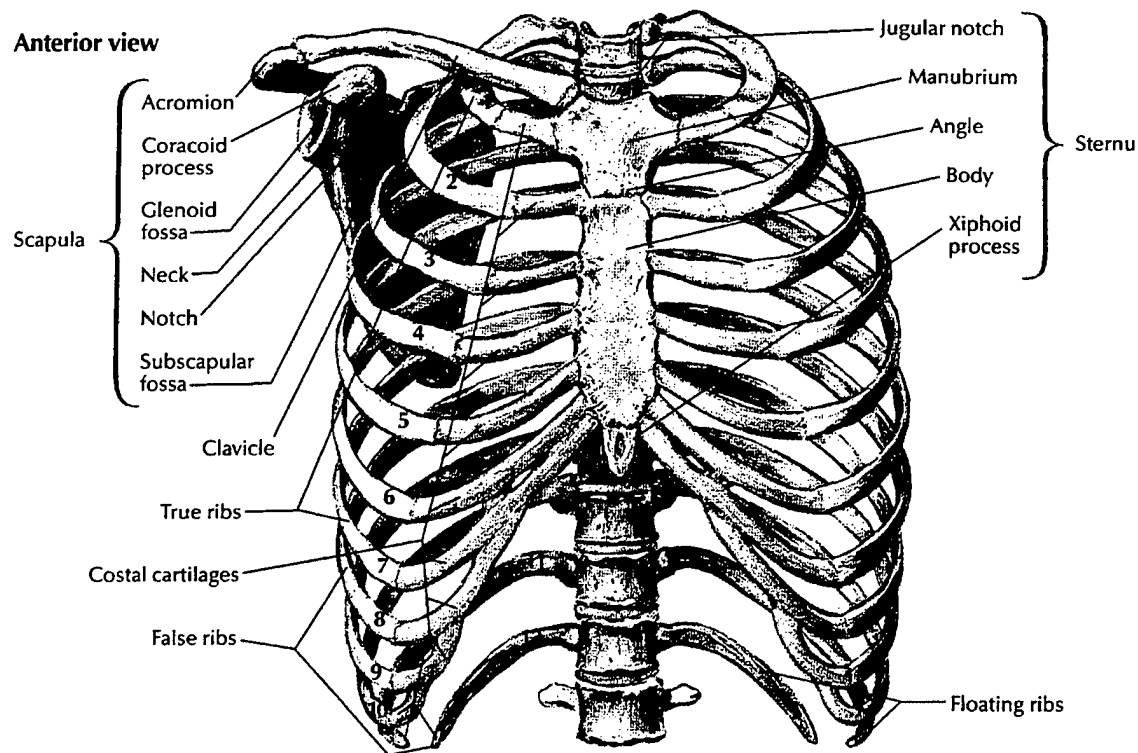
16

Figure 10. Skeletal Structure of the Thorax [Ref. 3]

Costal cartilage at the anterior and posterior ends of the ribs and at articulation points of the sternum and vertabrae have properties between that of compact bone and soft tissue such as muscle allowing for movement of the thorax to support respiratory functions.

3. Sternum

The sternum, subjected to non-penetrating impact load displaces essentially as a rigid body [Ref. 7]. The sternum consists of compact bone with the manubrium at the top and xiphisternal junction at the lower or anterior end of the sternum. The sternum is rigidily connected to the ribs via costacartilage of rib pairs 1 through 7. The sternum is depicted in Figure 11.
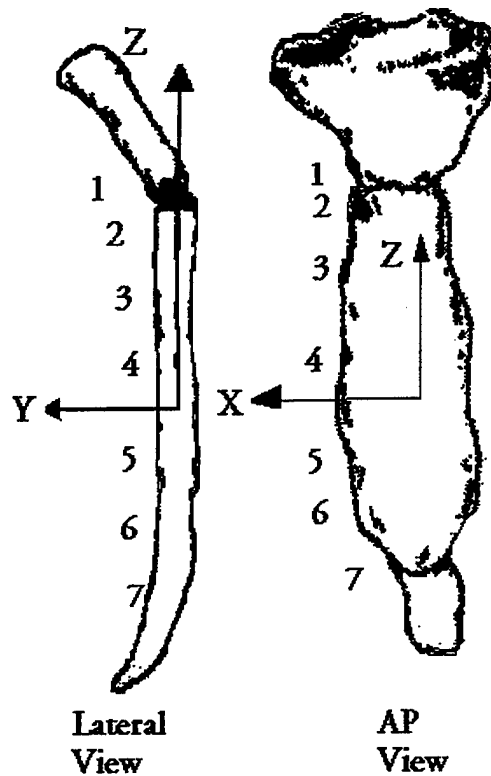
Figure 11. Structure of the Sternum[Ref. 10]

D. LITERATURE SURVEY

Reviewing literature, some similar studies have been done in the area of finite element analysis of the human thorax. Most of the preceding research has been restricted to the static analysis and attempt at validation of the finite element model. Literature involving the dynamic analysis of thoracic impact is not readily available in the literature. This study requires background information on the biomechanics of the human body, the characteristics of the human injury, and modeling technique, such as the finite element method. The literature survey was conducted in this regard.

The finite element method is a very popular technique for modeling the complex human body. There have been intensive studies on how to model the human body. Although extensive research has been conducted in the static finite element analysis, dynamic modeling is sparse in the literature but is used extensively in automobile impact testing and analysis.

Andriacchii, Schultz, Belytschko, and Galante [Ref. 8] developed a three dimensional model for the studies of the human thorax. The model was constructed from the model developed by Roberts and Chen [Ref .7]. The ribs were added to further understand the rib cage role in providing increased stiffness to the spine. The study was under taken to better understand the lateral stability of the spine due to scoliotic deformities. Details are provided in [Ref. 8].

Roberts and Chen [Ref .7] developed an elastostatic finite element model of the human thorax including the sternum, costal cartilage, ribs, and vertebra column to study the displacement and stress fields of the sternum, costal cartilage, and ribs and as a result of static loading or slowly applied loads. The material properties and geometry of the model developed is the basis of most of the later work conducted in finite element modeling of the human thorax. This model was used as a starting point for the finite element model developed for this study.

Yoganandan and Pintar [Ref. 13] conducted a study to determine the biomechanical material properties of thoracic spine and ribs from a large population. They determined material and geometric properties including, cross sectional area, moment of inertia, failure load, deflection and Young's modulus using three point bending techniques with a known force applied to isolated seventh and eighth rib pairs. Refer to [Ref. 13] for detailed results.

Belytschko, and Schwer [Ref. 10] developed a three dimensional model of the human spine, torso and head to evaluate mechanical response of pilot ejection. Rigid bodies were used to represent the vertebrae, pelvis, head, and ribs. These bodies were inter-connected by deformable bodies. The results are provided in [Ref. 10].

Kyusang [Ref .11] investigated the biomechanical response of the human body in a military vehicle due to pressure loading caused by a mine explosion. He developed a

model of the human body which extended the model King [Ref. 12] developed of the human head and cervical spine.

III. FINITE ELEMENT MODEL

A. HUMAN THORACIC BODY MODEL

The objective of this research was to evaluate the biomechanical response of the human thorax due to impact loading. Therefore, the FEM modeling of the human thorax was critical for this in this research. However, it was very difficult to model the details of the human body because of its complex geometry, material property, and wide variation of the geometry and material properties from person to person and age distribution. The finite element model developed for this study is depicted in Figure 12.
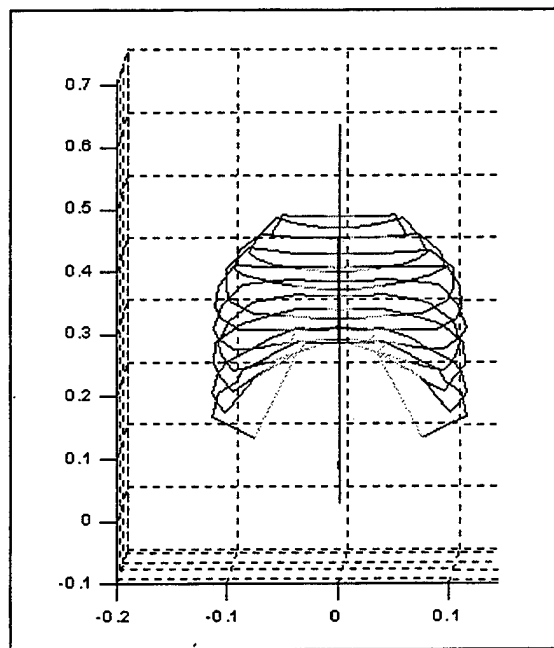

Figure 12. FEM Model of a Human Skeletal Thorax

Linear elastic behavior is assumed for all materials. Material properties in earlier studies and finite element approaches to the biomechanical behavior of the human thorax relied heavily on data obtained by crude measurement techniques and approximations. In order to develop a more a refined and more accurate finite model element the requirement to obtain more accurate biomechanical properties is needed. Yogananda [Ref. 13] determined the biomechanical properties of the seventh and eighth ribs by classical solid

21

mechanics approach of the three point bending experiments over a wide range of subjects. These material properties were used as a starting point for determining the material properties used in this study. Material properties for the vertabrae and discs were adopted from Sundaram [Ref. 9] and Belytschko [Ref. 10]. The compact bone material properties were adopted from Yogananda [Ref.13] and fitted to the data for each rib pair obtained from Roberts and Chen [Ref. 7]. The sternum material properties were assumed to be the same as for rib 4 compact bone. The material properties were varied along the height of the vertabral column as well along the length of each rib pair.

The finite element model developed consists of the cervical, thoracic, and lumbar spines, rib pairs 1 – 10, sternum and personnel protective equipment or bullet proof vest. The components include rib, cartilage, sternum, vertabrae, discs, facet joints, and connective elements representing the articulation between ribs and vertabrae. A total of 253 nodes and 397 individual beam elements were used to completely describe the skeletal model. Each vertabrae was modeled with two beam elements. Each vertabrae disc was modeled with one beam element. Facet joints are modeled as two beam elements extending from midpoints of adjacent vertabrae. Rib pairs one through ten are modeled with thirteen individual beam elements. This number of elements was considered essential to capture the entire rib including the head, tubercle, the angle, the midauxillary line junction, and costrachondral joint, and sternochondral junction. The sternum is modeled with seven individual beam elements in the midsaggital plane and fourteen individual beam elements in the XY plane. The three dimensional nodal data was adopted from Andriacchi [Ref. 8] and Roberts and Chen [Ref.7]. All of the data was extended to further capture the behavior of the human thorax and refine the finite element model.

B. PERSONNEL PROTECTIVE VEST

The finite element model of the personnel protective vest was modeled using a plate element consisting of 18 elements which covered the area of interest for the impact of the projectile. This allowed for analysis of plate bending and shear deformation with respect to the bullet impact including analysis of the plate deformation and corresponding

deformation of the modeled thorax. Plate bending and shear deformation are a result of the Mindlin/Reissner plate theory which includes the effect of transverse shear deformation. Unlike classical Kirchoff plate theory, a plane normal to the midplane before deformation does not remain normal to the mid-plane after

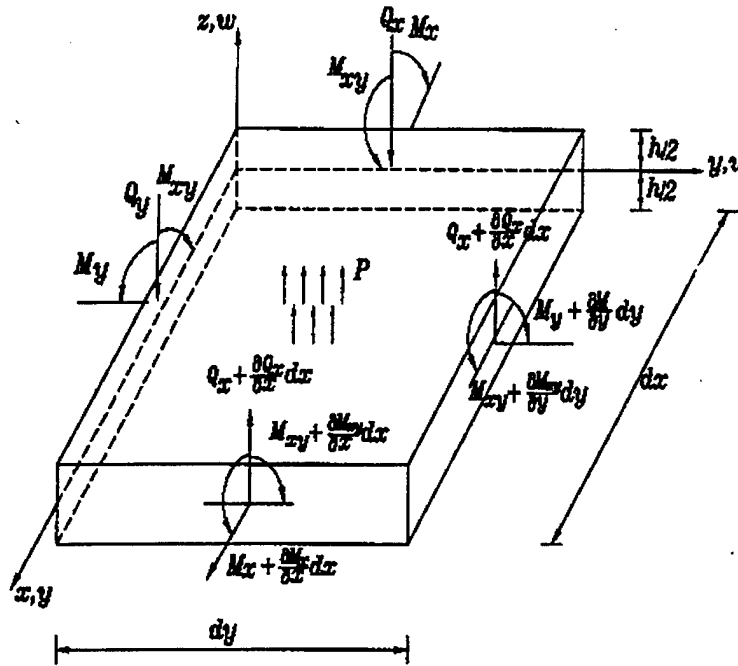deformation [Ref. 14]. Figure 13 is a free body diagram of the plate element.

Figure 13. Free Body Diagram of a Plate Element [Ref. 14]

The basic equations for classical plate theory are

$$\frac{\partial M_x}{\partial x} + \frac{\partial M_{xy}}{\partial y} - Q_x = 0$$

$$\frac{\partial M_{xy}}{\partial x} + \frac{\partial M_y}{\partial y} - Q_y = 0$$

$$\frac{\partial Q_x}{\partial x} + \frac{\partial Q_y}{\partial y} + p = 0$$

23

including the transverse shear forces. The element stiffness matrix for shear deformable plate bending is expressed as

$$[K^e] = \frac{h^3}{12} \int_{\Omega_e} [B_b]^T [D_b][B_b] d\Omega + kh \int_{\Omega_e} [B_s]^T [D_s][B_s] d\Omega$$

in order to derive the element stiffness matrix $[K^e]$ shown above we must express the strains in terms of nodal variables. The in-plane displacements are given by

$$u = -z\Theta_x(x,y)$$
$$v = -z\Theta_y(x,y)$$

the transverse displacement is

$$w = w(x,y).$$

For the shear deformable plate

$$\Theta_x = \frac{\partial w}{\partial x} - \gamma_{xz}$$

$$\Theta_y = \frac{\partial w}{\partial y} - \gamma_{yz}$$

where γ is the angle caused by the transverse shear deformation. The transverse deflection or displacement, w, and slope ,Θ, are independent, therefore shape functions are used to interpolate them.

The transverse and slope are interpolated as

$$w = \sum_{i=1}^{n} H_i(\xi,n)w_i$$

$$\Theta_x = \sum_{i=1}^{n} H_i(\xi,n)(\Theta_x)_i$$

$$\Theta_y = \sum_{i=1}^{n} H_i(\xi,n)(\Theta_y)_i$$

where n is the number of nodes and the shape functions used to interpolate the displacements are the same as those used to interpolate the slope. Bending and shear strains are computed from the displacements as follows

$$\{\varepsilon_b\} = -z[B_b]\{d_e\}$$
$$\{\varepsilon_s\} = -[B_s]\{d_e\}$$

24

where,

$$[B_b] = \begin{bmatrix} \dfrac{\partial H_1}{\partial x} & 0 & 0 & \dfrac{\partial H_2}{\partial x} & 0 & 0 & \dfrac{\partial H_3}{\partial x} & 0 & 0 & \dfrac{\partial H_4}{\partial x} & 0 & 0 \\[3mm] 0 & \dfrac{\partial H_1}{\partial y} & 0 & 0 & \dfrac{\partial H_2}{\partial y} & 0 & 0 & \dfrac{\partial H_3}{\partial y} & 0 & 0 & \dfrac{\partial H_4}{\partial y} & 0 \\[3mm] \dfrac{\partial H_1}{\partial y} & \dfrac{\partial H_1}{\partial y} & 0 & \dfrac{\partial H_2}{\partial y} & \dfrac{\partial H_2}{\partial y} & 0 & \dfrac{\partial H_3}{\partial y} & \dfrac{\partial H_3}{\partial y} & 0 & \dfrac{\partial H_4}{\partial y} & \dfrac{\partial H_4}{\partial y} & 0 \end{bmatrix}$$

is matrix representing the interpolation of the bending strains and

$$[B_s] = \begin{bmatrix} -H_1 & 0 & \dfrac{\partial H_1}{\partial x} & -H_2 & 0 & \dfrac{\partial H_2}{\partial x} & -H_3 & 0 & \dfrac{\partial H_3}{\partial x} & -H_4 & 0 & \dfrac{\partial H_4}{\partial x} \\[3mm] 0 & -H_1 & \dfrac{\partial H_1}{\partial y} & 0 & -H_2 & \dfrac{\partial H_2}{\partial y} & 0 & -H_3 & \dfrac{\partial H_3}{\partial y} & 0 & -H_4 & \dfrac{\partial H_4}{\partial y} \end{bmatrix}$$

is a matrix of shape functions representing the interpolation of the shear strains. The constitutive equations are given by

$$[D_b] = \frac{E}{1-v^2} \begin{bmatrix} 1 & v & 0 \\ v & 1 & 0 \\ 0 & 0 & \dfrac{1-v}{2} \end{bmatrix}$$

$$[D_s] = \begin{bmatrix} G & 0 \\ 0 & G \end{bmatrix}$$

E: Elastic modulus

v: Poisson's Ratio

G: Shear modulus

[D_b] and [D_s] are the constitutive equation for bending and shear and the displacements are

25

$$\{d_e\} = \{(\Theta_x)_1 \quad (\Theta_y)_1 \quad w_1 \quad (\Theta_x)_2 \quad (\Theta_y)_2 \quad w_2 \quad (\Theta_x)_3 \quad (\Theta_y)_3 \quad w_3 \quad (\Theta_x)_4 \quad (\Theta_y)_4 \quad w_4\}^T$$

C. INTERFACE ELEMENTS

To provide an interface between the ribs and spine, zero length or discrete elements were utilized. This same type of approach was also used in the connection of the plate and thorax model subassemblies to complete the system. The finite element code defines the discrete beam element for simulating the effects of a linear elastic zero length beam by using six springs each acting about one of the six local degrees of freedom. Each spring constant was adjusted depending on its allowable movement based on expected biomechanical behavior.

D. PROJECTILE MODEL

For this research a NATO 7.62 mm Ball M80 was utilized in the simulation of the projectile. The projectile was fired from a distance of approximately 13 meters from the target. The initial or muzzle velocity of approximately 3750 f/s (1143m/s) results in an impact velocity of 2575 f/s (784.86 m/s). The velocity loss (V_L) is a result of drag and relative air velocity and behaves as

$$V_l = \frac{XGD_{rel}}{C}$$

where

$X = meters\ to\ impact$

$G = Drag\ coefficent$

$D_{rel} = air\ density$

$C = ballistic\ coefficient$

There is no consistent result in the impact behavior of bullet striking a target. Because of the impossibility of controlling bullet strike and degree of penetration statistical approaches are necessary and the military services have established a V_{50}

ballistic limit [Ref. 15]. This is the minimum or maximum velocity at which a particular projectile is expected to completely penetrate the target or consistently fail to fully penetrate the armor given a thickness of the armor and material properties and angle of obliquity. This V_{50} ballistic limit was used to approximate the force of the bullet at impact.

The force of the impact can then be calculated by calculating the momentum based on mass and velocity of projectile. The time period of interest from impact to bullet coming to rest is approximately 100 μsec. The force upon impact is calculated based on the momentum and time.

$$Momentum = (mass_{bullet}) X (velocity_{bullet})$$

$$Momentum = .0080519 kg * 693.42 m/s$$

$$Momentum = 6.59 kg \cdot m/\sec$$

$$\int (Force) dt = Momentum$$

As the first approximation the forcing function and response is expected to be sinusoidal in shape. This model did not consider the penetrating capabilities of the bullet or hypervelocity projectile. The preliminary results of field experimentation indicate that the projectile did not fully penetrate the bullet-proof vest. The projectile did cause extensive trauma resulting in comminutation of the sternum. The projectile fully penetrated the ceramic armor but was stopped by the kevlar backing material. The expected forcing function applied to the bulletproof vest is depicted Figure 14.
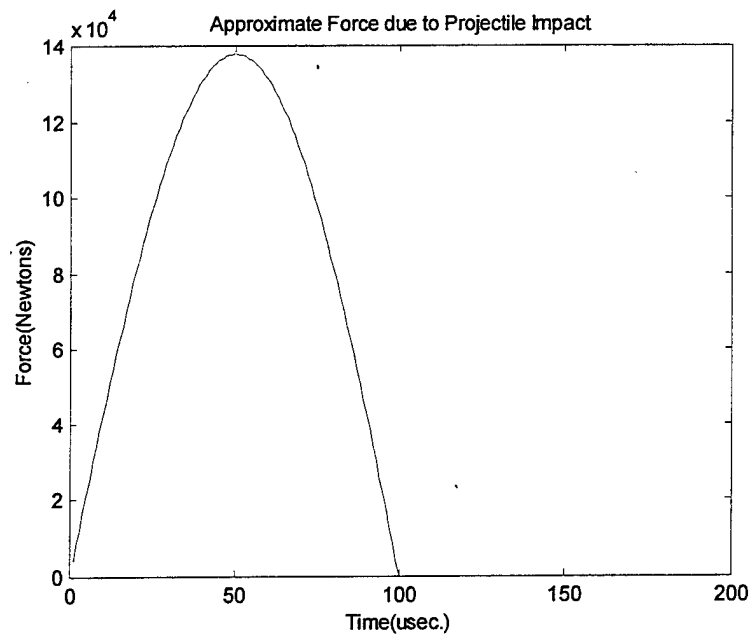
Figure 14. External Force

E. MODEL SOLUTION

An explicit stiffness method was used in the solution of the finite element model. This solution approach is based on the theory and practice described in The Finite Element Method using Matlab [Ref. 14]. MATLAB 5.2 was used to solve the matrix equations for the static study. C language was utilized to solve the transient analysis due to time considerations.

IV. INJURY ANALYSIS

There are no universal standard to evaluate injury potential of the human body caused by external loading, because everyone is different in size, strength, and even response to the same loading conditions. Differences also arise from sex, age, and body posture. However, consistent demands for evaluating injuries and protecting the human being from injuries were motivated and resulted in some injury criteria and reference values, which have been commonly used in the aerospace and automobile industry for safety. These are discussed here to provide some insight into the type and extent of injury that can occur due to a projectile strike to the protected area of the sternum.

Injury analysis is somewhat difficult in this case because the mechanism that produces the injury or the bullet impact is localized and non-linear which includes plastic flow around the impact sight as the bullet travels to rest. Several phenomena occur in and around the bullet strike. Local pettaling may occur which is plastic deformation of a ductile material when struck by an impacting projectile or fragment causing the material to be forced outward in leaflets or petal forms [Ref. 15]. Spalling, the detachment or delamination of a layer material in the area surrounding the location of the impact, can also occur due to bullet strike. Spalling can occur on either the front or rear surface and may produce injury even though bullet penetration is not complete. This is local behavior and was neglected because the interest is strictly in the overall displacement of the sternum. The focus of this research is trauma to the human thorax caused by a deflection or loading rate. In other words a basic assumption is that the protective body armor will stop the projectile prior to full penetration of the body armor.

Rib fracture and flail chest, excessive motion of the chest, occur due to frontal impact of the chest. It is most probable that the ribs fail due to bending on the tensile side of the rib. Rib fractures normally occur with chest deflection of over 3 inches, but no fractures occur at deflections of less than 2.3 inches. The number of rib fractures depends on the magnitude of the chest deflection [Ref. 16]. The amount of force depends on the rate of loading. Therefore at a given loading rate force appears to be related to the number of rib fractures due to the viscous nature of the thorax [Ref. 16].

The extent of lung contusion is velocity dependent. At very high velocities a compression wave is transmitted through the chest wall to the lung causing damage to the capillary bed of the alveoli (air sacs) [Ref .1]. Lung lacerations can occur at rib fracture sites.

Bleeding into the lung tissue or hemothorax can result due to injury to blood vessels as a result of rib fractures. Sucking chest wounds or pneumothorax results if the pleural sac is ruptured resulting in a hole. This type of injury is a result of deflection of the chest.

Heart and great vessel injuries can also occur in high speed thoracic impact. Just as the lungs the heart can be subject to contusions, lacerations as well as cardiac arrest. Contusions are a result of compression and the velocity of the compression. Cardiac lacerations are a result of sternum communication and high magnitudes of compression over the sternum. Heart fibrillation can occur at high rates of loading. The most serious of injuries other than direct communication of the projectile with the heart is aortic rupture. Large fluid pressures may cause a water hammer effect causing the vessel to rupture. Twisting or tearing caused by deformation or high internal pressures and may also cause rupture of the vessels.

Several scaling methods are used in the automobile industry to classify or scale injuries. These scaling techniques may not be appropriate for bullet impact but they do provide some insight into the survivability of the injury if the body armor of personnel protective equipment is successful in stopping the projectile. The result would be similar to blunt impact to the thorax. The Abbreviated Injury Scale (AIS) establishes a numerical rating system that ranges from 0 (no injury) to 6 (virtually unsurvivable). Table 1 provides an abbreviated AIS for the thorax. The table provides some insight into the extent of injury and survivability of personnel based on the injury.

Tolerance Level	Injury Level
Force	
3.3kN to sternum	Minor injury
8.8kN to chest and shoulders	Minor injury
Acceleration	
60 g's	3ms limit for hybrid II&III
Deflection(mm)	
58	No rib fracture
76	Limit for Hybrid III
Compression(%)	
20	Onset of rib fracture
40	Flail Chest
32	Tolerance for rib cage stability

Table 1. Frontal Impact Injury Tolerances. [Ref. 16]

V. RESULTS AND DISCUSSION

The human thorax model was first exposed to a static load applied at the sternum in order to provide some insight into the validity of the model. This was accomplished using MATLAB 5 and the results were compared to earlier studies. Earlier studies include experimental information and finite element modeling. The finite element model was then subjected to a transient load applied at the protective vest covering the sternum and compared to recent live-fire testing of instrumented cadavers. The finite element model was assembled with the use of ANSI C programming language because of the increased speed of the processing time. The MATLAB 5 files were translated to ANSI C language. The plate and thoracic body stiffness matrices were computed separately and then assembled into a system matrix. Acceleration, velocity, and displacement were computed using numerical integration scheme called the central difference technique

Of particular interest was the displacement of the sternum and subsequent displacement of the thoracic body resulting in applied stresses and strains of the internal organs such as the heart, lungs, liver, and other soft tissue. Although not specifically modeled, damage to internal organs is readily apparent in the displacement field of the sternum and rib cage and laceration injury may result due to rib fracture sites.

A. STATIC ANALYSIS

Literature describing the static loading of the human thorax provided an avenue for the initial model validation and was used in the static phase of this research. Initially, a static or quasistatic force was applied to provide some measure as to the model usefulness.

Two loading cases were considered. A 100lb (444.82 kg.) load was applied to the mid-sternum line and a 50lb (222.41) point force applied at rib two. The global system stiffness matrix was formed. Boundary conditions appropriate for the simulation were then applied. In this case, the boundary conditions simulated a cadaver lying on a table. The nodes corresponding approximately to the position of the ribs that extend posteriorly

the farthest distance out were pinned. This normally corresponds to a position between the angle and tubercle of each rib pair.

The global displacement were obtained and used in an initial validation process of the model. The displacement field of the sternum was evaluated and compared to the experimental and numerical studies of Andricchii [Ref.16], Nahum [Ref.16], and work done by Patrick [Ref.16] with embalmed cadavers and fresh cadavers (males and females). The static loading results compared favorably with the embalmed cadavers as well as the earlier numerical models of Andricchi. Figure 15 provides a qualitative comparison between the model developed and earlier models as well as a comparison between the developed model and earlier analysis of a static or quasi-static force applied to fresh and embalmed cadavers.
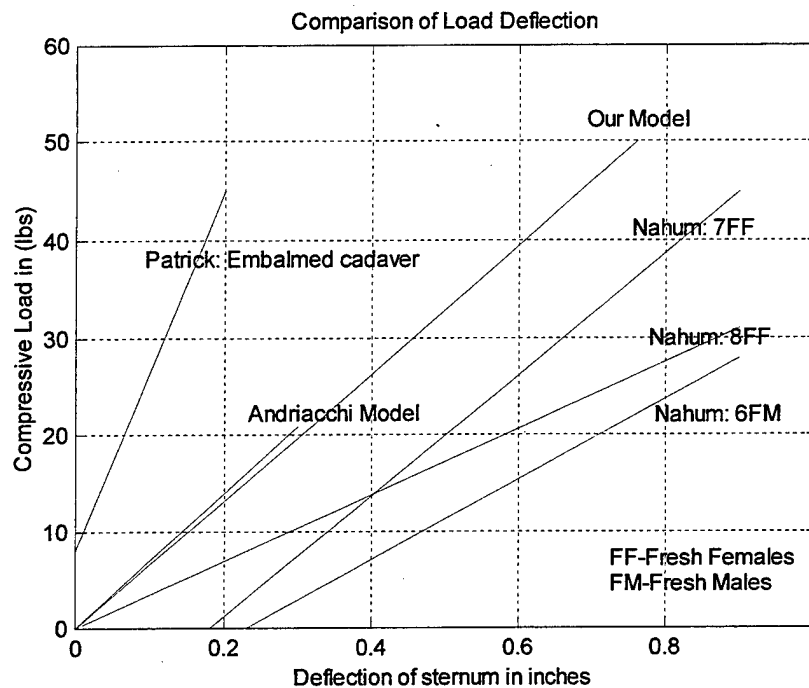

Figure 15. Comparison of Thoracic Load Deflection Curves [After Ref.9]

The anterior to posterior displacement of the sternum is shown in Figure 16 as a result of the 100lb load. The deflection of sternum and the deflection of the individual ribs pairs 1 though 7 are shown in figures 17 – 23 as a result of 100lb load.
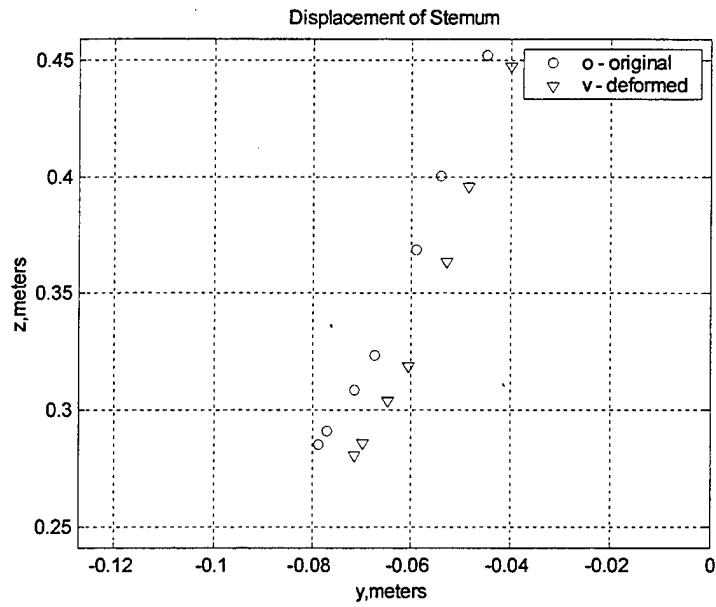
34

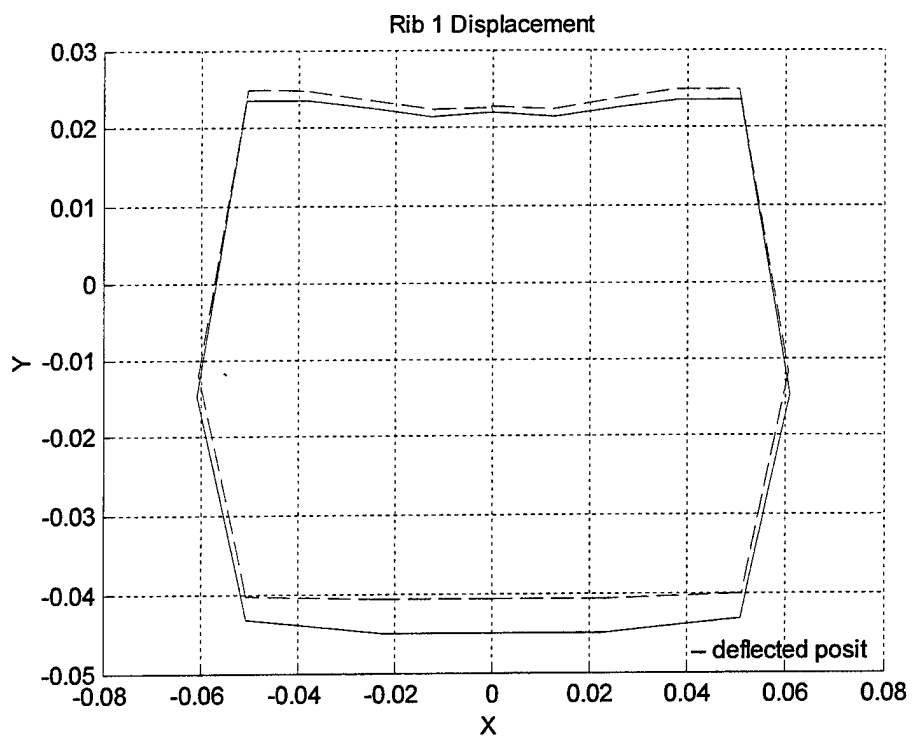Displacement of Sternum

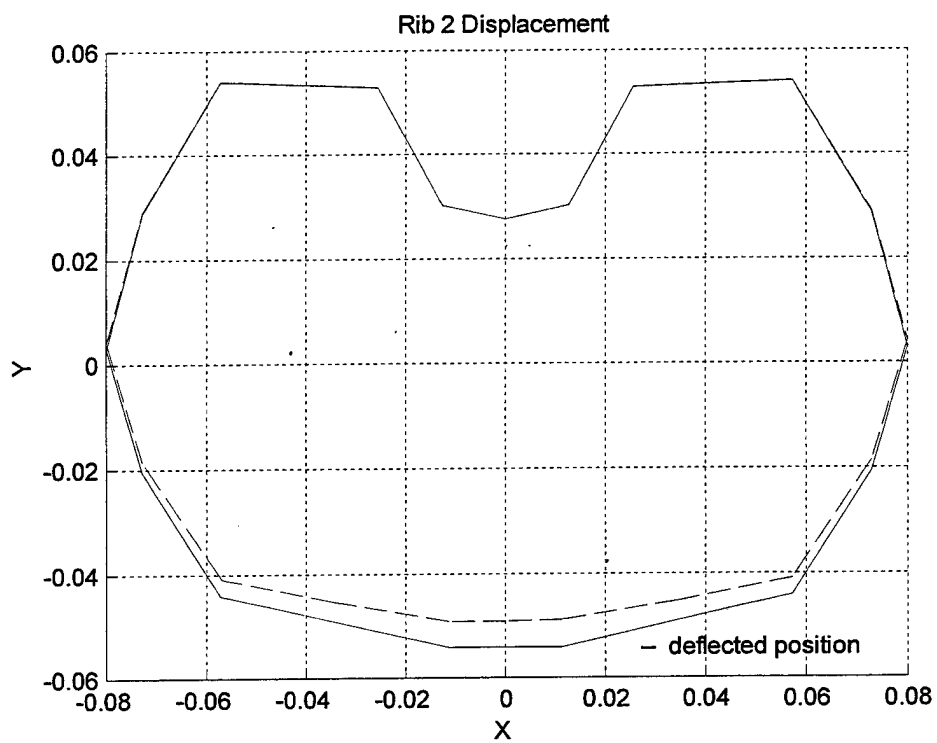**Figure 16. Sternum Deflection**

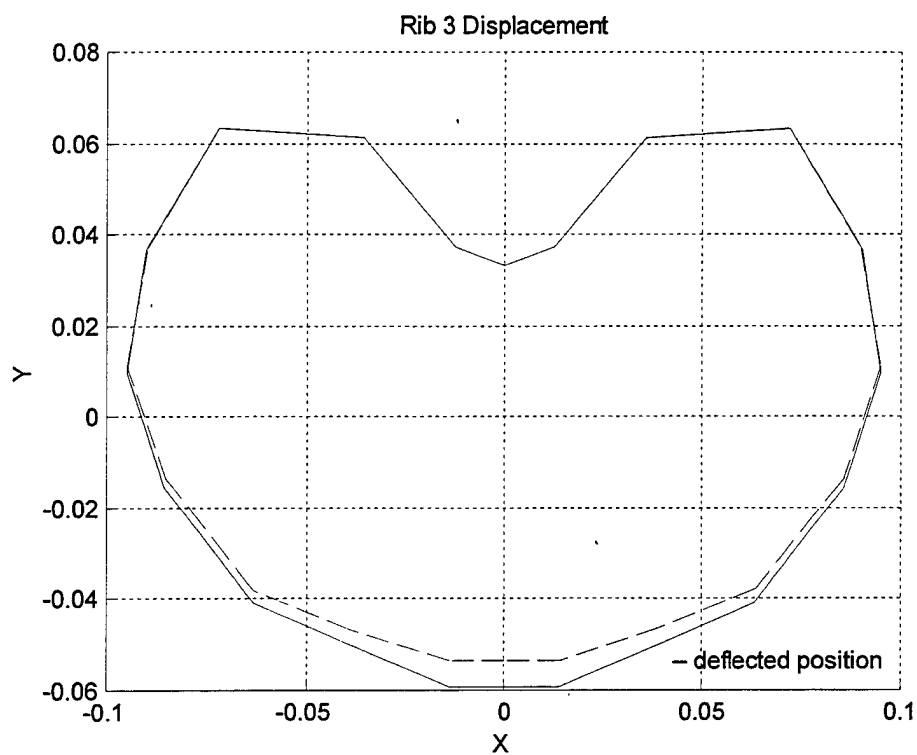**Figure 17. Rib 1 Deflection**

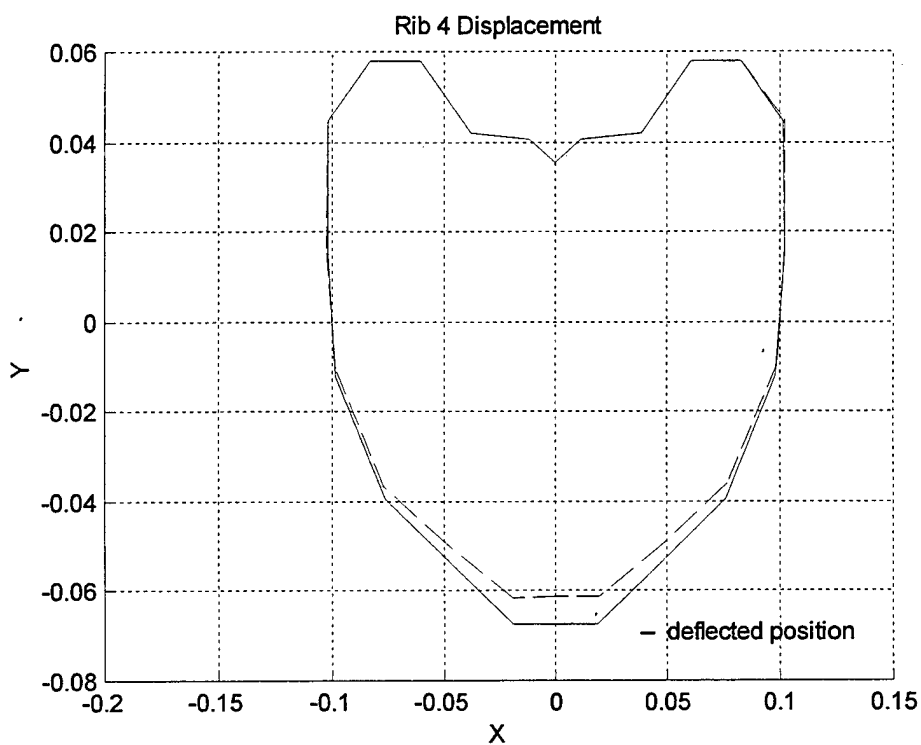**Figure 18. Rib 2 Deflection**

Figure 19. Rib 3 Deflection

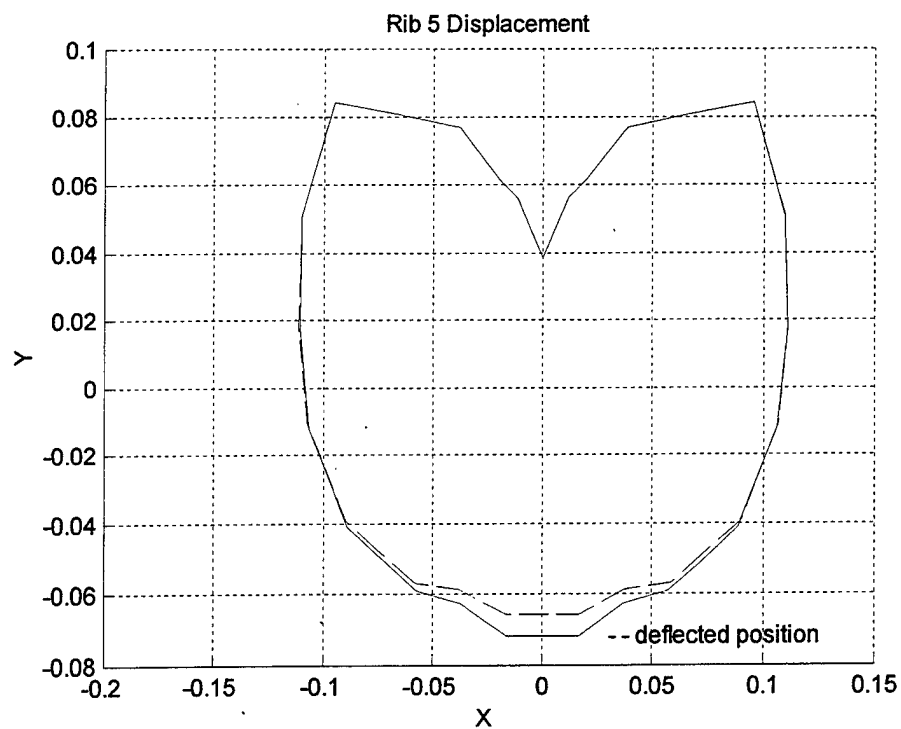**Figure 20. Rib 4 Deflection**

37

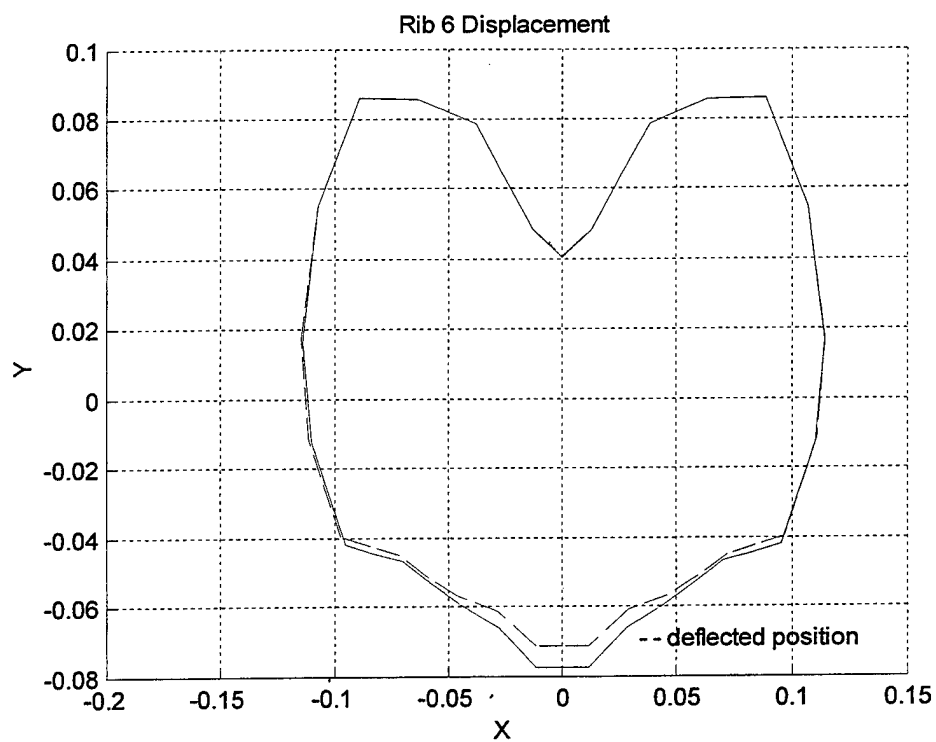**Figure 21. Rib 5 Deflection**

Figure 22. Rib 6 Deflection

38
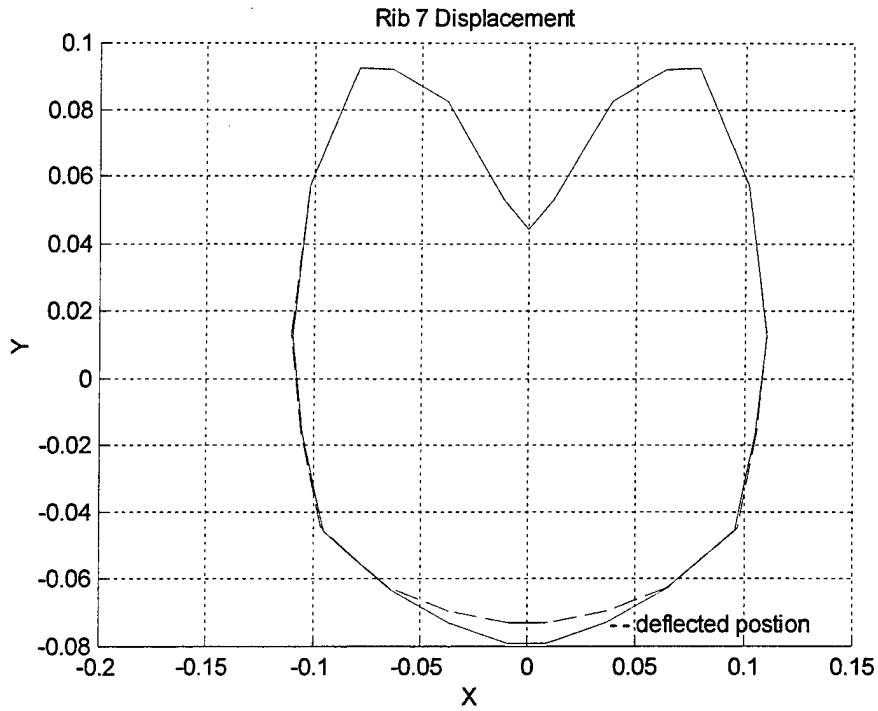
Figure 23. Rib 7 Deflection

Once the displacements are found at each node, local or elemental forces are determined. Stress and strain was obtained by the use of transformation equations from global displacements to local displacements. This resulted in obtaining the local force vector at each node and then the corresponding stresses through well-known strength of materials theory. The derivation is included below

$$global\{displacement\} \rightarrow local\{displacement\}$$

$$\{displacement\}_{local} \equiv \begin{Bmatrix} u \\ v \\ w \\ \Theta_x \\ \Theta_y \\ \Theta_z \end{Bmatrix}_{node}$$

$$\{Force\} = [k]_{element} \, x \{displacement\}_{local}$$

39

$$\{Force\} = \begin{Bmatrix} F_x \\ F_y \\ F_z \\ M_x \\ M_y \\ M_z \end{Bmatrix}_{nodal}$$

The theory of solid mechanics or mechanics of materials approximates the stresses at each node in the following manner:

$$\sigma_{axial} = \frac{F_x}{Area}$$

$$\sigma_{bending} = \frac{M_y z}{I_y} + \frac{M_z x}{I_z}$$

$$\tau = \frac{M_x r}{J}$$

where :

$\sigma = stress$

$M = Moment$

$I = moment\ of\ inertia$

$\tau = shear\ stress$

$J = polar moment\ of\ inertia$

The maximum axial tensile stresses in the bony rib elements for the applied load of 100 lbs. along the midsternum line are given in Table 2. These axial stresses found in previous study by Roberts and Chen are included in Table 2 for comparison.

Location	Present model σ_{axial}	R&C model σ_{axial}
Rib 1	74.4Mpa	59.9Mpa
Rib 2	12.62Mpa	18.47Mpa
Rib 3	65.85Mpa	18.86Mpa
Rib4	54.28Mpa	23.25Mpa
Rib5	43.78Mpa	27.94Mpa
Rib6	34.23Mpa	25.14Mpa
Rib7	31.5Mpa	46.66Mpa

Table 2. Tensile Stress

The maximum tensile stresses observed in our finite model compare relatively well with the maximum stress computed in the finite element model study conducted by Roberts and Chen [Ref. 7]. There are several reasons for the variations in tensile stresses including model geometry, material properties, and boundary conditions. In the Roberts model only rigid connections were used between elements. The model also assumed that the material properties did not change significantly between elements. The modeled spine did not include the vertabrae discs or flexible joint connection between the vertabrae and rib pairs. The model developed for this study was much more refined. The material properties used were based on experimentally obtained material properties found by three point bending experiments conducted by Yogananda [Ref. 13]. Geometry was extensively refined adding flexible joint to model articulation of the rib and spine. The spine includes vertabrae, vertabrae discs, and facet joints.

The Roberts and Chen study did not analyze the bending stress in the thoracic body. To provide some assurance as to the validity of the model concerning bending stresses an anterior posterior 50 lb. load was applied to the sternum at rib 2 vertical position. Sundaram and Feng [Ref. 9] used a similar loading in the finite element model developed in 1975. In this comparison the axial stress and two bending stresses were summed to obtain a total stress. The maximum computed stress for each rib and the maximum stress found by Sundaram and Feng are provided in Table 3.

41

Location	Present model σ_{max}	S&F model σ_{max}
Rib 1	70.33Mpa	67.96Mpa
Rib 2	15.18Mpa	32.00Mpa
Rib 3	21.48Mpa	36.04Mpa
Rib 4	24.2Mpa	28.92Mpa
Rib 5	61.86Mpa	9.10Mpa
Rib 6	36.12Mpa	21.86Mpa
Rib 7	25.35Mpa	23.96Mpa

Table 3. Maximum Stress

The maximum stresses also compared relatively well with the finite element model constructed by Sundaram [Ref. 9]. The model constructed by Sundaram was a full thoracic body including gross models of the heart and lungs and muscle tissue. The Sundaram model adopted similar properties and geometry to that of the Roberts model. The addition of the viscera, and muscle allowed for an attendant decrease in stress in the Sundaram model as expected.

B. TRANSIENT ANALYSIS

The human thorax was outfitted with a plate to simulate a bulletproof vest covering the sternum and surrounding chest area. The impact was simulated as a NATO 7.62 round striking the plate at the number three rib vertical position. Newton's law dictates that momentum must be conserved. Therefore a projectile striking the human body must transfer its momentum to the body. The size of a NATO 7.62 round or its mass requires it to travel at high velocities to deliver the momentum required to knock a person down. The high velocity of the bullet or projectile means it will penetrate the body causing considerable trauma. Body armor must be able to convert the momentum of the bullet by deforming it sufficiently to slow it down enough that the impact will be similar to a blunt blow to the body.

Recent live fire tests conducted at U.S. Army Aberdeen Test Center, Aberdeen Proving Ground, Maryland using cadavers outfitted with new boron carbide ceramic armor indicate accelerations of the sternum of up to 1500g's or 14,715m/s^2 as a response to a NATO 7.62 ball round hitting a ceramic armor vest in front of the chest. The corresponding accelerations of the trachea, aorta, and the spine were 500g's, 200g's, and 20g's respectively.

The goal of the research is to approximate this acceleration by the use of the finite element model created. There are a great number of assumptions made in the creation of the finite element model due to the amount of real life information that was unknown or unavailable. These are cadaver material properties, boron carbide vest properties, the applied force due to impact, and instrumentation irregularities associated with position and orientation and fixation techniques of the accelerometers and other instrumentation.

Figure 24 depicts computed via the finite element method and measured acceleration as a result of the projectile impact during tests conducted on 18 June 1999.
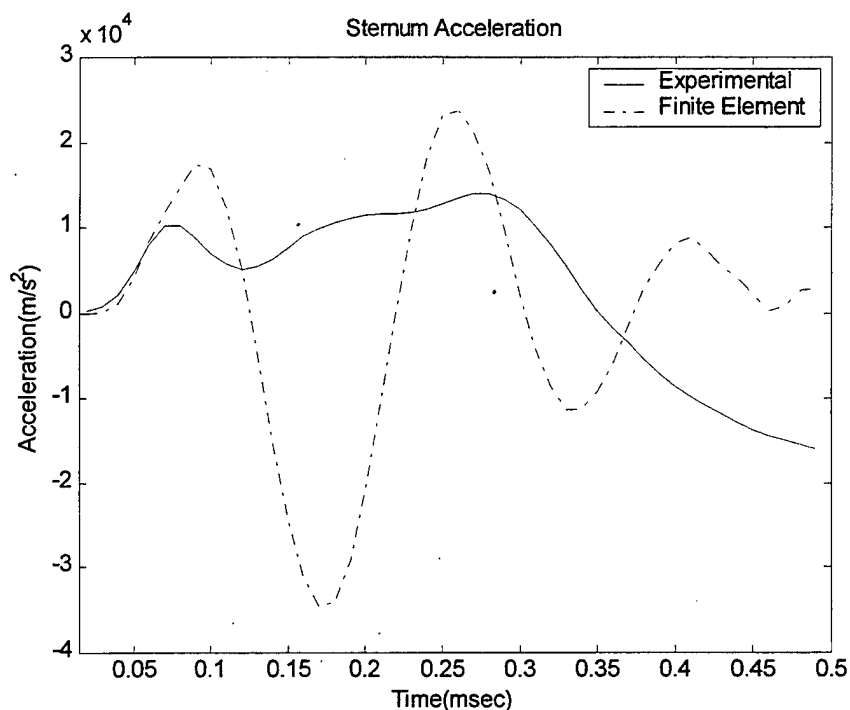

Figure 24. Sternum Acceleration

A simple study of varying the velocity with a subsequent variation of the applied force was also attempted using the finite element model. The projectile was changed to a 9mm projectile similar to that used in the United States Armed forces and by NATO forces as well. The 9mm projectile is a 124 grain with an approximate impact velocity of one-half that of the NATO 7.62 projectile. A comparison of the sternum acceleration based on NATO 7.62 round and the 9mm round is given in Figure 25.
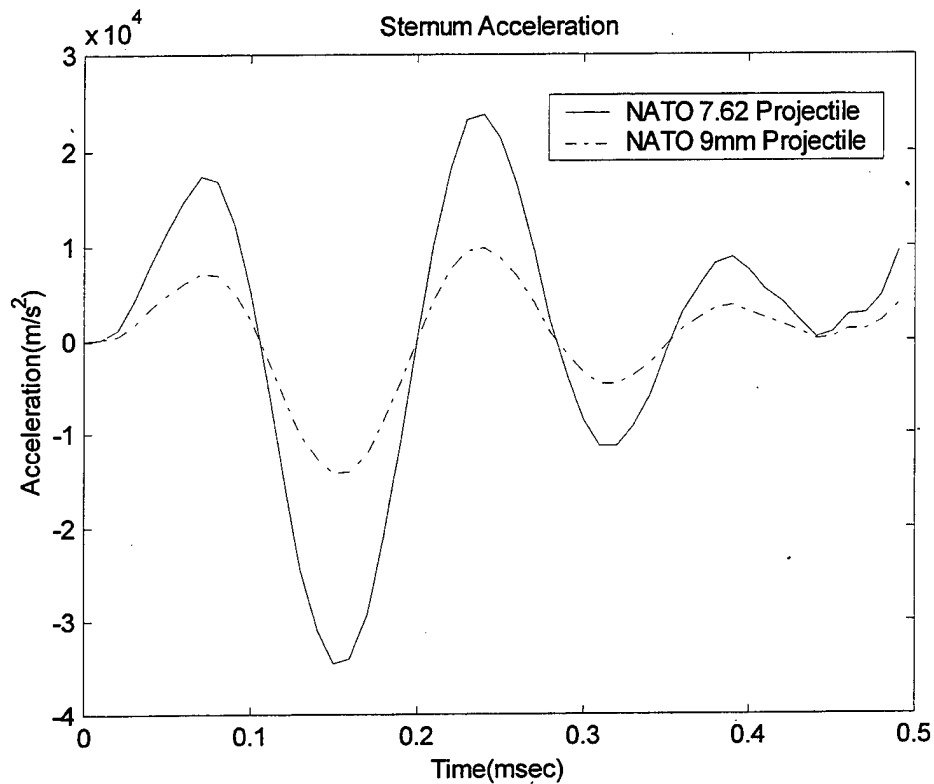

Figure 25. Sternum Acceleration

VI. CONCLUSIONS AND RECOMMENDATIONS

A. CONCLUSIONS

This research is an effort to use the classical solid mechanics approach coupled with a numerical solution technique to predict the response of a structure to an excitation. This research investigated both the static and transient biomechanical response of the human thorax to an impact. The static analysis of the finite element model provided an avenue to meet an initial validation objective. This provided a jumping off point to attempt a much more difficult dynamic analysis.

The static analysis shows a favorable comparison of the finite element model developed and earlier work in both experimental studies using cadavers and finite element modeling of the spine. Several differences are evident in comparing the present model to previous finite element models. These include material properties, and geometry. In the earlier studies the material properties of the bony ribs and cartilage were virtually unknown and based only on experimental data obtained from studies using long bones such as the femur. A typical value was used for the entire bony model as well as for the cartilage and soft tissue. All connections were assumed rigid with no allowances provided for movement of the rib cage relative to the spine. Due to the computation time required in earlier studies the models included only a limited number of elements in both the spine and rib cage.

The present model includes 397 beam elements. Each element varies in material properties based on the most recent experimental data available. The bony rib material properties were based on large population experiments conducted to obtain the material properties of the bony rib pairs. The number of elements used in the present model more accurately reflects the human thorax. Discrete elements were used where appropriate to model the connection between the subassemblies of the entire system. These elements allowed for more movement that more accurately reflects the movement of the thorax.

The dynamic model response seen in Figure 24 accurately predicts the response of the sternum initially but then oscillates around the experimental results. The finite

element response is predictable in that no muscle or internal organs were included in the model. The added muscle and internal organs would have provided some of the necessary damping to more accurately predict the response. The force used to excite the model was unknown from the "live fire" experiments. Engineering sense predicts some type of sinusoidal excitation to model the impact force. The angle of obliquity of the projectile strike was assumed to be zero. The impact obliquity due to a fired projectile is varies substantially from one impact to the next. This variation causes dramatic changes in the crater volume of the ceramic armor caused by the projectile. This further effects the velocity of the bullet through the armor. The oscillatory response is predictable in that no internal organs or muscle were included in the model. The added soft tissue should provide some of the necessary providing a more accurate description of the response. The material properties of the ceramic armor were also unknown due to proprietary constraints. MIL-P- 64513 was used for the description of the boron carbide ceramic armor used by the military today in ceramic armor plating. The above assumptions allow for some inaccuracy in the model response and clearly effect the oscillatory nature seen in the response. It is also clear that initially the finite element model closely matches the experimental results. As the stress wave is transmitted through the vest and is felt at the sternum the viscoelastic effects due to collagen components such as muscle, tendons ligaments and cartilage is negligible and the accelerations of the finite element model sternum and the cadaver sternum are similar. After the point where the collagen fibers begin to straighten out or extend the viscoelastic effects become a major influence in the behavior of the sternum. This behavior is believed to cause what appears to be a damped response in the cadaver.

B.   RECOMMENDATIONS

In conducting this research, many problems arose, including modeling a human body associated with its material and mechanical properties, experimentation versus computer simulation, and assumptions assocciated with the experimental process

The following recommendations need to be incorporated in subsequent resesearch in order to improve the reliability of the computer modeling and simulation:

- Further analysis of the material properties of the rib compact bone and cartilage is needed.

- An investigation into the biomechanical behavior of the costa vertabral joint that focuses on the material properties associated with the joint and the articulation process of the ribs with the spine to include the possibility of a dual connection needs to be conducted.

- The finite element model must be refined to include soft tissue including muscle, internal organs, ligaments, and tendons.

- Validation of the assumptions in the experimental results needs to be conducted. These include applied force, boundary conditions, geometry and material properties of the vest, and instrumentation location and orientation.

LIST OF REFERENCES

1. Fung Y.C., *Biomechanics: Mechanical Properties of Living Tissue*, Springer-Verlag, New York, 1993.

2. Nordin, M. and Frankel, V., Basic Biomechanics of the Musculoskeletal System, Williams and Wilkins, 1989.

3. Netter, Frank H., *Atlas of Human Anatomy*, CIBA-Geigy Corporation, 1989

4. Augustus, A. and Manohar, M., *Clinical Biomechanics of the Spine*, second edition, Lippincott-Raven Publishers, NewYork, Philadelphia, 1990.

5. Albert, Damon, et al., *The Human Body in Equipment Design*, Havard University Press, Cambridge, Massachusetts, 1966.

6. Calais-Germain,B., *Anatomy of Movement*, Eastland Press, Seattle, WA, 1993.

7. Roberts, S. B. and Chen, P.H. *Elastostatic Analysis of the Human Thoracic Skeleton.* J. Biomechanics vol 3, 1970.

8. Andriacchi, T., Shultz, A., Belytschko, T., and Galante, J., *A Model for the Studies of the Mechanical Interaction Between the Human Spine and Rib Cage.* J. Biomechanics vol 7 1974.

9. Sundaram, S.H. and Feng,C.C., *Finite Element Analysis of the Human Thorax.* J. Biomechanics vol 10, 1977.

10. Belytschko, T., Schwer, L., and Privitzer, E., *Theory and Application of a Three Dimensional Model of the Human Spine*, Aviation, Space, and Environmental Medicine, January 1978.

11. KyuSang L., *Biomechanical Response of the Human Body inside a Military Vehicle Exposed to Mine Explosion*, Thesis, Naval Postgraduate School, Monterey, CA, March 1999.

12. King, Q.M., *Investigation of Biomechanical Response due to Fragment Impact on Ballistic Projective Helmet*, Thesis, Naval Postgraduate School, Monterey, CA, March 1998.

13. Yogananda, N. and Pintar F.A., *Biomechanics of Human Thoracic Ribs*, Journal of Biomechanical Engineering vol 120, 1998.

14. Kwon, Y. W. and Hyochoong Bang, *The Finite Element Method Using MATLAB*, CRC Press 1997.

15. Military Standard V50 Ballistic Test for Armor, MIL-STD-622E January 1987.

16. Nahum, A.M. and Melvin J. *Accidental Injury: Biomechanics and Prevention,* Springer-Verlag New York, 1993.

INITIAL DISTRIBUTION LIST

No. Copies

1. Defense Technical Information Center..2
   8725 John J. Kingman Rd., STE 0944
   Ft. Belvoir, VA 22060-6218

2. Dudley Knox Library...2
   Naval Postgraduate School
   411 Dyer Rd.
   Monterey, CA 93943-5101

3. Professor Young W. Kwon, Code ME/Kw..2
   Department of Mechanical Engineering
   Naval Postgraduate School
   Monterey, CA 93943

4. Engineering & Technology Curricular Office (Code34)...............................1
   Naval Postgraduate School
   Monterey, CA 93943

5. Department of Mechanical Engineering..1
   Naval Postgraduate School
   Monterey, CA 93943

6. Timothy A. Hughes/LT/US Navy...2
   4374 Belmont Rd.
   Tchula, MS 39169